Spectral decomposition of time- vs. depth-migrated data

Tengfei Lin, the University of Oklahoma; Zhonghong Wan, BGP Inc., CNPC; Bo Zhang, Shiguang Guo and Kurt Marfurt, the University of Oklahoma; Yi Guo, China University of Petroleum*

Summary

Spectral decomposition is a powerful analysis tool that has been significant success in delineating channels, fans, overbank deposits and other relative thin architectural elements of clastic and carbonate depositional environments. Because of its success in fluvial-deltaic and basin floor turbidite-fan systems, most publications of spectral decomposition have used time-migrated data. Interpreting spectral components and spectral attributes such as peak frequency on depth migrated data requires a slightly different perspective. First, the results are computed as cycles/km (or alternatively as cycles/1000 ft) rather than as cycles/s or Hertz, with the dominant wavenumber decreasing with increasing velocities at depth. Second, interpreters resort to depth migration when there are significant lateral velocity changes in the overburden and/or steep dips. All present-day implementations compute spectral components vertical trace by vertical trace rather than perpendicular to the bedding plane, giving rise to tuning and other anomalies at an apparent rather than at a true frequency or wavenumber.

We illustrate the interpretational differences of spectral decomposition between time- and depth-migrated data through the use of a simple synthetic model and a modern 3D data volume. We show how one can approximately compensate for reflector dip by normalizing each spectral magnitude component by $1/\cos\theta$, where θ is the volumetric dip magnitude commonly computed in seismic attribute analysis

Introduction

Seismic attributes have been applied to depth-migrated data since their inception. Since the dominant wavelength increases with increasing velocity which in turn increases with depth, attributes such as coherence benefit by using shorter vertical analysis windows in the shallow section and longer vertical analysis windows in the deeper section. Since most coherence implementations require a fixed vertical analysis window, the interpreter simply runs the algorithm using an appropriate window for each zone to be analyzed. Curvature is naturally computed in the depth domain, with most algorithms requiring a simple conversion velocity for time-migrated data. For more accurate results, the interpreter uses different conversion velocities for different target depths, or simply converts the entire volume to depth using well control. Both coherence and curvature are structurally driven algorithms, with coherence computed along structural dip and curvature computed from structural dip.

In contrast, spectral decomposition is computed trace by trace which implicitly ignores any dipping structure. One of the most common uses of spectral decomposition is to map shallow (e.g. Partyka et al., 1999; Peyton et al., 1998) and deepwater (e.g. Bahorich et al., 2002) stratigraphic features using a simple thin bed tuning model. Widess (1973) used a wedge model and found maximum constructive interference occurs when the wedge thickness equals the tuning thickness (one-half of the two-way travel-time period for time-migrated data or one-quarter of the wavelength for the depth-migrated data). Using this model, Laughlin et al. (2002) shows that deeper channels are stronger at lower frequencies, while the shallower flank of the channel has stronger amplitudes at higher frequencies. Although this is the most common use of spectral decomposition, spectral components are currently the method of choice in estimating attenuation (1/Q), pore-pressure prediction, and seismic unconformities, as well as some implementations of seismic chronostratigraphy.

Theory

Short-window Discrete Fourier Transform (SWDFT), Continuous Wavelet Transforms, and Matching Pursuit

There are currently three algorithms used to generate spectral components: short-window discrete Fourier transforms (SWDFT), continuous wavelet transforms, and matching pursuit. Leppard et al. (2010) find that matching pursuit provides greater vertical resolution and less vertical stratigraphic mixing than the other techniques. For this reason, all our examples here will be generated using a matching pursuit algorithm described by Liu and Marfurt (2007). However, the concept of apparent vs. true frequency is perhaps easiest to understand using the fixed length analysis window used in the SWDFT. For time data, the window will be in seconds, such that the spectral components are measured in cycles/s or Hz. For depth data, the window will be in kilometers, such that the spectral components are measured in cycles/km. Significant care must be made when loading the data into commercial software, where the SEGY standard stores the sample interval in microseconds. For everything to work correctly, a depth sample interval of 10 m will need to be stored as

DOI http://dx.doi.org/10.1190/segam2013-1166.1

10000 "microkilometers". If the units are not stored in this manner, the numerical values of the data may appear to be in fractions of a cycles/m. Many commercial software packages will not operate for cycles/s (or cycles/km) that fall beyond a reasonable numerical range of 1-250.

Once the data are loaded, the range of values will be different. If the time domain data range between 8-120 Hz, depth domain data will range between 2-30 cycles/km at a velocity of 4 km/s, such that anomalies will be shifted to the lower "frequencies".

Volumetric dip and its influence

If the dip angle is θ, and the real thickness h_r, then the apparent thickness $h_a = h_r / \cos\theta$ (Figure 1). The tuning frequency (and tuning wavenumber) will therefore decrease with increasing values of θ. The shift to lower apparent frequency is familiar to those who examine data before and after time migration, where dipping events on unmigrated stacked data with moderate apparent frequency "migrate" laterally to steeper events with lower apparent frequency.

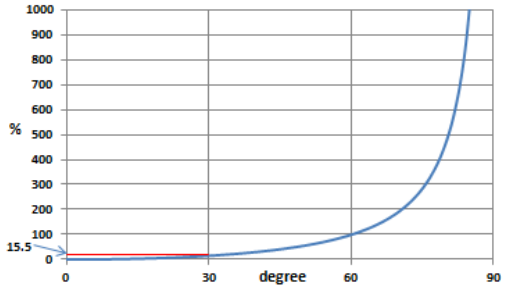

Figure 1. The percent change in apparent thickness h_a/h_r with respect to dip magnitude, θ.

Most volumetric dip computations provide apparent dips along the survey axes, θ_x and θ_y, which in turn define the unit normal, **a,** (Figure 2 where

$$a_x = \sin\theta \cos\emptyset, \quad (1)$$

$$a_y = \sin\theta \sin\emptyset, \quad \text{and} \quad (2)$$

$$a_z = \cos\theta, \quad (3)$$

where θ is the dip magnitude and $\emptyset$ is the dip azimuth.

The first eigenvector of dip estimates of the gradient structure tensor provides a direct estimate **a**. Other workers compute instantaneous frequency, ω, and wavenumbers, k_x and k_y, or use a semblance dip scan to compute apparent dips p and q measured in s/m.

$$\theta_x = \tan^{-1}\left(\frac{k_x}{k_z}\right); \quad \theta_y = \tan^{-1}\left(\frac{k_y}{k_z}\right) \quad (4)$$

$$\theta = \tan^{-1}\left[\frac{(k_x^2+k_y^2)^{\frac{1}{2}}}{k_z}\right]$$

$$= \tan^{-1}\left(\tan\theta_x{}^2 + \tan\theta_y{}^2\right) \quad (5)$$

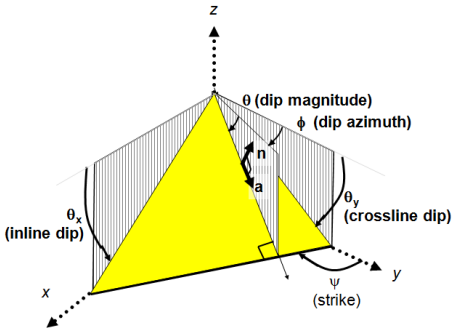

Figure 2. The definition of reflector dip. (After Marfurt, 2006).

If the earth can be approximated by a constant velocity, v, the relationships between apparent time dips p and q, and the apparent angle dips θ_x and θ_y, are

$$p = 2\tan\theta_x / v = k_x/\omega, \quad (6)$$

$$q = 2\tan\theta_y / v = k_y/\omega, \quad (7)$$

$$\cos\theta = \sqrt{\frac{1}{1+p^2+q^2}} \quad (8)$$

A synthetic example

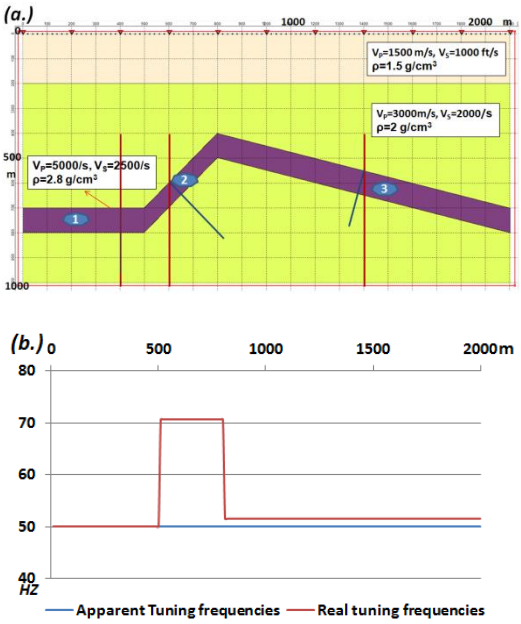

DOI http://dx.doi.org/10.1190/segam2013-1166.1

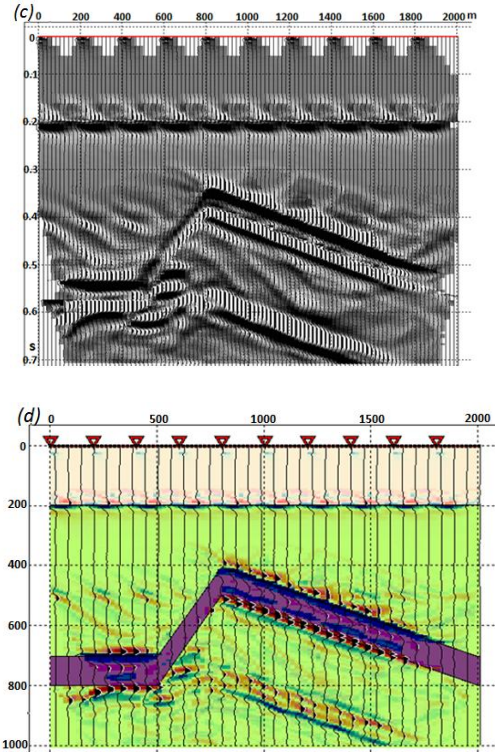

Figure 3. (a) A thin bed model showing layers components with (1) flat dip (2) strong dip to the left, and (3) moderate dip to the right. (b) The apparent (in blue) and real (in red) tuning frequency of the layer. (c) Synthetic seismic data generated by prestack time migration and stacking a suite of shot gathers. The deeper event is a multiple. (d) The peak frequency of (c) computed using a matching pursuit algorithm. Note the peak frequency (50Hz) in the layer corresponds to the apparent frequency in (b).

In Figure 3a, the vertical thickness of the thin bed is 100 m; the tuning frequency should be 50 Hz considering the velocity is 5000 m/s. The apparent thickness is constant across the model when measured vertically (blue curve in Figure 3b) such that spectral analysis results in a constant value of f_{peak} 50 Hz rather than the variable peak frequency given by the red curve in Figure 4b. Correcting the apparent thickness by $1/\cos\vartheta$ gives the correct answer. We generated a suite of shot gathers for the model shown in Figure 3a, migrated them, and then stacked the result, giving the vertical section shown in Figure 3c. We then computed the peak frequency using a matching pursuit spectral decomposition. Note the constant value of 50 Hz through the variable thickness layer.

Real Data Example

The real data are from an oilfield of east China. There are lots of fault-controlled reservoirs, exhibiting strongly on the seismic profile shown on both the time migrated and depth migrated data in Figure 4. The blue color cover the same position in both profiles, we found that the horizons are much deeper in depth migrated data than the ones in time migrated data. This is because the increase of velocity with time (depth).

The migrated data are sampled at Δt=0.002 s in time and Δz=0.01 km in depth. Figure 5 shows the average spectra of the data shown in Figure 4.

We compute the 3D dip and azimuth of the data and co-render it with seismic amplitude in Figures 6a and 7a. We also compute the peak spectral frequency using a matching pursuit algorithm and display the results in Figures 6b and 7b. Finally, we normalize the peak frequency by dividing by $1/\cos\theta$ and display the results in Figure 6c and 7c. As expected, the values of peak frequency are unchanged in areas of low dip but change significantly in areas of high dip (block arrows).

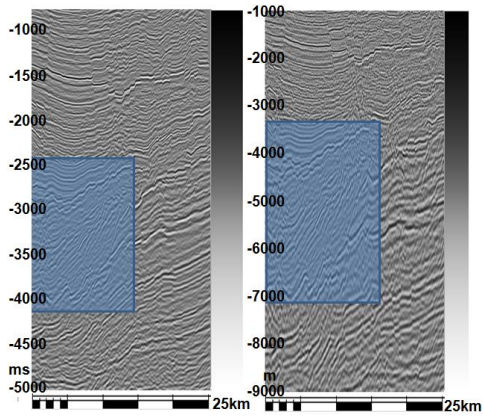

Figure 4. Seismic profile of time migrated data (left) and depth migrated data (right).

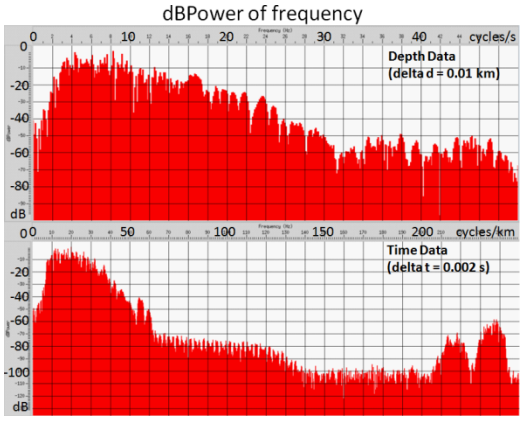

Figure 5. Average spectra of the (top) depth-migrated and (bottom) time-migrated data shown in Figure 4. Note the numerical range of 2-24 cycles/km for the depth migrated data in cycles/km is numerically lower than the 5-50 Hz range for the time migrated data. Even if the original seismic data were

DOI http://dx.doi.org/10.1190/segam2013-1166.1

bandlimited to 10-100 Hz, migration shifts the apparent spectrum to values below 10 Hz for steeply dipping events.

Conclusions

Spectral decomposition is a powerful analysis tool in mapping lateral variation in thin stratigraphic features at or below seismic resolution. Unfortunately, lateral variations in structural dip ϑ give rise to changes in apparent frequency that overprint the geological signal of interest. Time migration will shift the spectra to frequencies lower than that of the input unmigrated data in areas of steep dip. Such interpretational artifacts can be partially compensated by normalizing the spectrum by $1/\cos\vartheta$. Spectral decomposition works equally well for depth and time-migrated data, with tuning frequencies in Hz being replaced by tuning wavenumbers in cycles/km..

Acknowledgements

We thank BGP-CNPC for permission to use their data and the sponsors of the OU Attribute-Assisted Processing and Interpretation Consortium for their financial support.

EDITED REFFERENCES

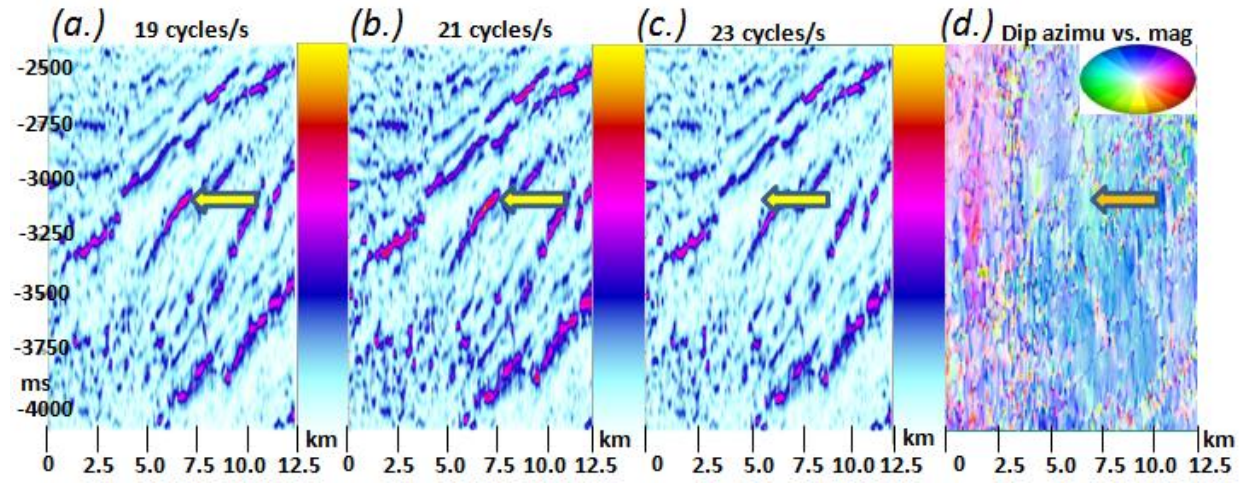

Figure 6. Analysis of time-migrated data shown in Figure 4(left). The frequency decomposition results (a. 19 cycles/s; b, 21cycles/s; c. 23 cycles/s) and dip azimuth vs. dip magnitude plot for the object pointed by the arrow in time migrated data

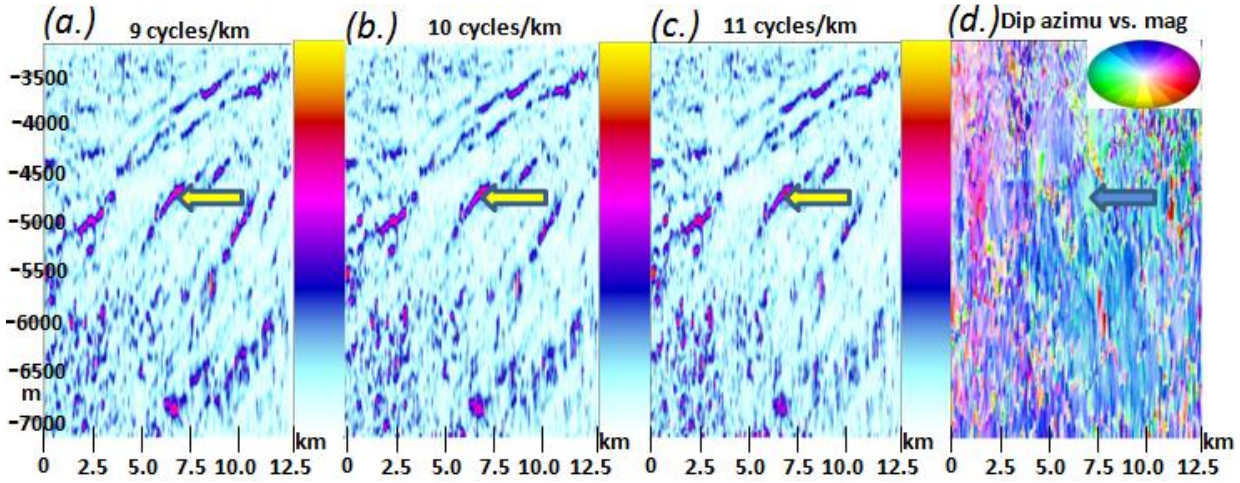

Figure 7. Analysis of time-migrated data shown in Figure 4(right). The frequency decomposition results (a. 9 cycles/km; b, 10 cycles/km; c. 11 cycles/km) and dip azimuth vs. dip magnitude plot for the object pointed by the arrow in depth migrated data

DOI http://dx.doi.org/10.1190/segam2013-1166.1

http://dx.doi.org/10.1190/segam2013-1166.1

EDITED REFERENCES

Note: This reference list is a copy-edited version of the reference list submitted by the author. Reference lists for the 2013 SEG Technical Program Expanded Abstracts have been copy edited so that references provided with the online metadata for each paper will achieve a high degree of linking to cited sources that appear on the Web.

REFERENCES

Bahorich, M., A. Motsch, K. Lauthlin, and G. Partyka, 2002, Amplitude responses image reservoir: Hart's E&P, January, 59–61.

Laughlin, K., P. Garossino, and G. Partyka, 2002, Spectral decomp applied to 3D: AAPG Explorer, http://www.aapg.org/explorer/geophysics_corner/2002/05gpc/cfm, accessed 9 April 2005.

Hoecker, C., and G. Fehmers, 2002, Fast structural interpretation with structure-oriented filtering: The Leading Edge, **21**, 238–243, http://dx.doi.org/10.1190/1.1463775.

Leppard, C., A. Eckersley, and S. Purves, 2010, Quantifying the temporal and spatial extent of depositional and structural elements in 3D seismic data using spectral decomposition and multiattribute RGB blending: 30th Annual GCSSEPM, Foundation Bob F. Perkins Research Conference, 1–10.

Liu, J. L., and K. J. Marfurt, 2007, Instantaneous spectral attributes to detect channels: Geophysics, **72**, no. 2, P23–P31, http://dx.doi.org/10.1190/1.2428268.

Marfurt, K. J., R. L. Kirlin, S. H. Farmer, and M. S. Bahorich, 1998, 3D seismic attributes using a running window semblance-based algorithm: Geophysics, **63**, 1150–1165. http://dx.doi.org/10.1190/1.1444415.

Partyka, G., J. Gridley, and J. A. Lopez, 1999, Interpretational applications of spectral decomposition in reservoir characterization: The Leading Edge, **18**, 353–360, http://dx.doi.org/10.1190/1.1438295.

Peyton, L., R. Bottjer, and G. Partyka, 1998, Interpretation of incised valleys using new 3D seismic techniques: A case history using spectral decomposition and coherency: The Leading Edge, **17**, 1294–1298, http://dx.doi.org/10.1190/1.1438127.

Widess, M. B., 1973, How thin is a thin bed?: Geophysics, **38**, 1176–1180, http://dx.doi.org/10.1190/1.1440403.